Inorganic Chemistry

Article

pubs.acs.org/IC

High-Concentration Na Doping of $SrRuO_3$ and $CaRuO_3$

Hayato Seki,[†] Ryuta Yamada,[†] Takashi Saito,[†] Brendan J. Kennedy,[‡] and Yuichi Shimakawa*[,†,§]

[†]Institute for Chemical Research, Kyoto University, Uji, Kyoto 611-0011, Japan

[‡]School of Chemistry, The University of Sydney, NSW 2006, Australia

[§]Japan Science and Technology Agency, CREST, Uji, Kyoto 611-0011, Japan

ABSTRACT: The Na-doped perovskite-structure ruthenates $Sr_{1-x}Na_xRuO_3$ and $Ca_{1-y}Na_yRuO_3$ were prepared by high-pressure synthesis, which enables us to go beyond the previously reported Na doping limits and substitute Na for over 50% of the Sr in $SrRuO_3$ and the Ca in $CaRuO_3$. Gradual and systematic changes in the crystal structures were observed, and the decreases in the Ru−O bond lengths confirmed the Na substitution at the *A* site caused hole doping to Ru^{4+} at the *B* site. In contrast to what has been previously reported, $Sr_{1-x}Na_xRuO_3$ showed metallic conductivity. Magnetic properties were influenced by the Na substitution, but no long-range antiferromagnetic behavior was observed in $Ca_{1-y}Na_yRuO_3$.

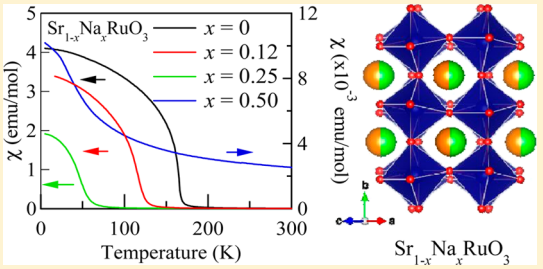

INTRODUCTION

Perovskite-type ruthenates have been drawing considerable attention for more than five decades because of their unusual magnetic and transport properties. $SrRuO_3$, which has a near metrically cubic structure but is actually orthorhombic in space group *Pnma*, is a metal and exhibits ferromagnetic behavior below 160 K.[1−4] Ferromagnetism in 4d transition-metal oxides is quite rare, and $SrRuO_3$ is an example of highly correlated electrons in narrow d bands giving rise to unusual properties. Indeed, optical spectroscopy measurements have suggested that $SrRuO_3$ has a non-Fermi-liquid-like electronic structure.[5,6] The analogous compound $CaRuO_3$ also crystallizes with a $GdFeO_3$-type distorted (*Pnma*) perovskite structure and is a metal.[1,4] The magnetic properties of $CaRuO_3$ remain controversial even after prolonged and extensive studies.[7] Some investigators have reported antiferromagnetic ordering, whereas several studies concluded that there is no long-range magnetic ordering in $CaRuO_3$ down to low temperatures.[3,8−10]

Cation substitution is typically used to change the physical properties of a compound by modulating its crystal, and hence electronic, structure. Apparently minor structural distortions can lead to significant changes in the magnetic and transport properties, as is well documented in the solid solution, $Sr_{1-x}Ca_xRuO_3$.[11,12] In that system isovalent substitution at the *A* site of the perovskite structure results in dramatic changes in the physical properties described above for $SrRuO_3$ and $CaRuO_3$. Conversely, aliovalent cation substitution at the *A* site alters, in the absence of anion vacancies, the filling of the d bands as well as inducing structural distortions. Substitution of monovalent Na for the divalent ions at the *A* site in $SrRuO_3$ and $CaRuO_3$ have been reported.[13,14] Suppression of ferromagnetism was observed in single-crystal $Sr_{0.88}Na_{0.12}RuO_3$ and in polycrystalline $Sr_{0.81}Na_{0.19}RuO_3$. Ceramic $Sr_{0.81}Na_{0.19}RuO_3$ showed metallic conductivity, whereas $Sr_{0.88}Na_{0.12}RuO_3$ was reported to be insulating. $Ca_{0.95}Na_{0.05}RuO_3$, on the other hand, remained in a metallic state, but an apparent antiferromagnetic-like transition at 55 K was observed in the temperature dependence of its magnetic susceptibility.[13] It does not appear to be possible to prepare more heavily Na doped samples using conventional solid-state synthetic methods. Evidently oxidation of the Ru^{4+}, induced by the aliovalent substitution of Na^+, has a significant impact on the properties of these oxides; however there are inconsistencies in the previous reports of the Na-doping effects, and the doping-induced changes in the crystal structure and the magnetic and transport properties were not fully investigated.

The recent reports of extraordinarily high antiferromagnetic transition temperatures in $SrTcO_3$ and $CaTcO_3$ are further illustration of the unusual physical properties that occur as a consequence of highly correlated electrons in narrow 4d bands.[15−17] Prior to this recent discovery, high Neel temperatures in oxides had only been observed for the first-row (3d) transition metals. The d^3 electron configuration of the Tc^{4+} cation appears to be a critical requirement for the observed magnetic properties. Doping $SrRuO_3$ with another d^3 ion, Cr^{3+}, increases T_C slightly, whereas all other dopants decrease T_C. It has been postulated that the d^3 electron configuration of Cr favors hybridization with the t_{2g} band of Ru^{4+}, broadening the bandwidth of this and consequently increasing T_C. High Neel temperatures have also been reported for some Ru^{5+} oxides that have a d^3 electron configuration.[18] There is considerable current interest in extending the family of heavy 4d transition-metal oxides displaying high magnetic ordering temperatures, and Ru^{5+} oxides, which will be isoelectronic with Tc^{4+}, are an attractive target, with $NaRuO_3$ being an obvious choice.

In the present study, we have prepared several $SrRuO_3$ and $CaRuO_3$ samples with various Na doping concentrations. Using

Received: February 2, 2014
Published: April 14, 2014

   dx.doi.org/10.1021/ic500265t | *Inorg. Chem.* 2014, 53, 4579−4584

a high-pressure synthesis technique, we were able to obtain Na doping levels greater than 50% in both systems, although we could not prepare pure $NaRuO_3$. Detailed changes in the crystal structure and the magnetic and transport properties of $Sr_{1-x}Na_xRuO_3$ and $Ca_{1-y}Na_yRuO_3$ are presented. This represents the first comprehensive study of the synthesis, structure, and magnetic and electric properties of heavily Na doped $SrRuO_3$ and $CaRuO_3$.

EXPERIMENTAL SECTION

It was impossible to obtain the more highly Na-doped samples by synthesis at ambient pressure. Consequently polycrystalline samples of $Sr_{1-x}Na_xRuO_3$ and $Ca_{1-y}Na_yRuO_3$ were prepared by solid-state reaction under high-pressure and high-temperature conditions using a DIA-type cubic anvil press. The synthesis in a confined capsule helped ensure the target cation compositions in the present experiments because it kept Na from being lost by evaporation.

Polycrystalline samples with nominal compositions of $Sr_{1-x}Na_xRuO_3$ (x = 0, 0.12, 0.25, 0.50, and 0.75) and $Ca_{1-y}Na_yRuO_3$ (y = 0, 0.10, 0.20, and 0.50) were prepared by solid-state reaction. Stoichiometric amounts of $SrCO_3$($CaCO_3$) and Ru metal powders were first well mixed and calcined at 1273 K for 12 h in air. The obtained powders were mixed with Na_2O_2, sealed in a gold capsule, and treated at 6−9 GPa and 1173 K for 30 min. The pressure was not released until the samples had cooled to room temperature. Some samples were mixed with an excess of Na_2O_2, and after the reaction the residual Na_2O_2 was removed by washing with distilled water. Note that Na_2O_2 produces a strong oxidizing atmosphere during the high-pressure and high-temperature reaction.

Phase identification and crystal structure analysis were conducted using synchrotron X-ray diffraction (SXRD). The room-temperature SXRD pattern produced at a wavelength of 0.773166 or 0.774565 Å was collected with a large Debye−Scherrer camera with an image plate at beamline BL02B2 in SPring-8. Each sample was packed into a glass capillary 0.1 mm in diameter that was rotated during the measurement. The obtained diffraction data were analyzed by the Rietveld method using the program RIETAN-FP.[19] Magnetic properties of the samples were measured using a SQUID magnetometer (MPMS, Quantum Design). Temperature dependence of magnetic susceptibility was evaluated by measuring the susceptibility in a 1 kOe magnetic field at temperatures from 5 to 300 K. The electrical resistivity of each sample was measured at temperatures from 5 to 300 K by a standard four-probe method using a Quantum Design PPMS.

RESULTS

$Sr_{1-x}Na_xRuO_3$. Figure 1a shows the SXRD patterns of $Sr_{1-x}Na_xRuO_3$ (x = 0.12, 0.25, and 0.50) recorded under ambient conditions. Even with the exceptional peak shape resolution of the SXRD patterns there was no obvious splitting of the stronger Bragg reflections indicative of orthorhombic symmetry. This reflects the high pseudosymmetry of the cell metric, and consequently we identified the appropriate space group through examination of the weak reflections associated with displacements of the anions. For each of the samples peaks indicative of both in-phase and out-of-phase rotations of the corner-sharing RuO_6 octahedra were observed, demonstrating the structures to be orthorhombic in *Pnma*. The diffraction patterns of the x = 0.12 and 0.25 samples suggest that both of the samples were single phase. As shown in Figure 2 the observed SXRD pattern for the x = 0.25 sample is well fitted by Rietveld refinement in *Pnma*, which is the same crystal structure observed for $SrRuO_3$. The refined Na occupancies for the x = 0.12 and 0.25 samples were 0.134(2) and 0.278(2), which are very close to the designed compositions. Refinements in which the occupancy of the two anion sites was allowed to vary did not provide any evidence for the presence of anion

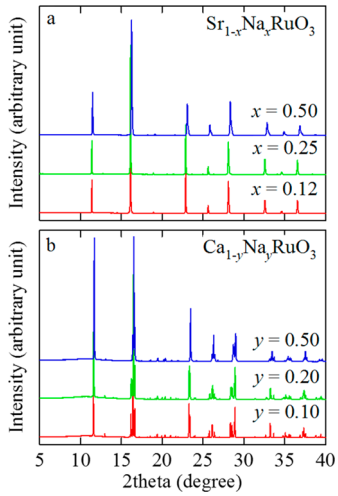

Figure 1. SXRD patterns for (a) $Sr_{1-x}Na_xRuO_3$ (x = 0.12, 0.25, and 0.50) and (b) $Ca_{1-y}Na_yRuO_3$ (y = 0.10, 0.20, and 0.50).

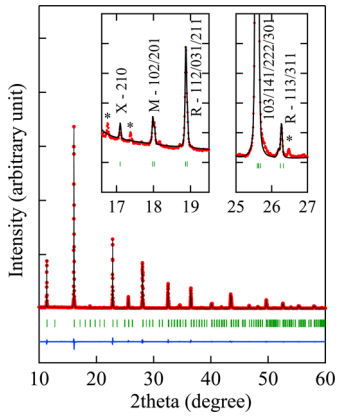

Figure 2. SXRD pattern and the Rietveld analysis results for the nominal $Sr_{0.75}Na_{0.25}RuO_3$ sample. The observed (circles), calculated (line), and difference (bottom line) patterns are shown. The ticks indicate the positions of Bragg reflections. The inset highlights the presence of the superlattice reflections associated with the cooperative titling of the octahedra. The R-point reflections are associated with out-of phase tilts and the M-point reflections with M-phase tilts. The X-point reflections occur when both tilt types are present. The asterisks represent impurity peaks.

vacancies, and together with the fact that samples were prepared under strongly oxidizing conditions, let us to conclude that these were fully occupied in the final refinements. The diffraction peaks of the x = 0.50 sample, on the other hand, showed broadening of all the reflections, including the weak superlattice reflections, to higher angles, indicating a phase mixture. The observed diffraction pattern was well reproduced by a two-phase model with slightly different lattice constants. The result of the Rietveld refinement clearly shows that the x = 0.50 sample consists of two phases with slightly different Na doping concentrations: 73.8%-$Sr_{0.539(3)}Na_{0.461(3)}RuO_3$ and 26.2%-$Sr_{0.333(5)}Na_{0.667(5)}RuO_3$. Attempts to prepare $Sr_{0.75}Na_{0.25}RuO_3$ were unsuccessful. The results of the structure analysis are listed in Table 1. The lattice constants of $Sr_{1-x}Na_xRuO_3$ decrease with increasing Na concentration as shown in Figure 3a, and as a result, the volume of the sample also gradually decreases (Figure 3b), confirming the systematic substitution of Na at the Sr site. With increasing Na doping, the

dx.doi.org/10.1021/ic500265t | *Inorg. Chem.* 2014, 53, 4579−4584

Table 1. Refined Structural Parameters, Selected Bond Lengths, Bond Angles, and Ru Bond Valence Sums (BVS) for $Sr_{1-x}Na_xRuO_3$ and $Ca_{1-y}Na_yRuO_3$[a]

Sr_{1-x} Na_x RuO3		x = 0	x = 0.12	x = 0.25	x = 0.50	
a (Å)		5.532 83	5.52057(3)	5.50197(2)	5.4635(2)	5.4284(2)
b (Å)		7.847 12	7.83091(5)	7.80301(5)	7.7483(1)	7.7114(5)
c (Å)		5.569 26	5.55273(3)	5.52484(3)	5.4761(1)	5.4467(2)
A occupancies	Sr	1	0.866(2)	0.722(2)	0.539(3)	0.333(5)
	Na	0	0.134	0.278	0.461	0.667
Ru−O (Å)	(×2)	1.99	2.000(5)	1.995(4)	1.983(8)	2.01(3)
	(×2)	1.98	1.970(5)	1.950(5)	1.948(8)	1.87(3)
	(×2)	1.978	1.979(1)	1.972(1)	1.956(2)	1.948(7)
Ru−O−Ru angle (deg)		165.1	163.3(3)	163.3(3)	160.0(4)	163.6(7)
		162.1	160.8(3)	162.4(2)	159.3(3)	163.8(5)
volume (Å^3)		241.799	240.050(2)	237.192(2)	231.817(9)	228.00(2)
BVS for Ru		4.02	4.02	4.13	4.25	4.53
R_{wp} (%)			6.156	5.506	6.552	
R_p (%)			4.258	3.690	4.092	
ψ (deg)		9.0	9.6(2)	8.8(1)	10.4(5)	8.1(3)
φ (deg)		7.5	8.4(2)	8.4(2)	10.0(2)	8.2(4)
$Ca_{1-y}Na_yRuO_3$		y = 0	y = 0.10	y = 0.20	y = 0.50	
a (Å)		5.524	5.50154(3)	5.48696(5)	5.42056(4)	
b (Å)		7.649	7.63980(4)	7.63404(6)	7.60278(5)	
c (Å)		5.354	5.34668(3)	5.34668(5)	5.33809(4)	
A occupancies	Ca	1	0.892(7)	0.766(1)	0.450(6)	
	Na	0	0.108	0.234	0.550	
Ru−O (Å)	(×2)	2.002	1.994(5)	1.996(6)	1.982(4)	
	(×2)	1.990	1.979(4)	1.951(6)	1.936(4)	
	(×2)	1.979	1.978(1)	1.973(2)	1.953(1)	
Ru−O−Ru angle (deg)		149.9	149.9(3)	150.7(3)	153.4(2)	
		148.9	149.8(2)	151.7(3)	152.3(2)	
volume (Å^3)		226.22	224.725(2)	223.960(3)	219.990(3)	
BVS for Ru		3.93	4.01	4.12	4.31	
R_{wp} (%)			8.863	9.309	5.752	
R_p (%)			6.403	6.515	4.256	
ψ(deg)		15.6	15.1(1)	14.2(2)	13.9(2)	
φ(deg)		15.1	15.1(1)	14.7(2)	13.3(1)	

[a]All values obtained from the structure analysis with SXRD. Space group is *Pnma*. Numbers in parentheses are standard deviations of the last significant digit. The data for $SrRuO_3$ (x = 0) are from ref 23, and the data for $CaRuO_3$ (y = 0) are from ref 24.

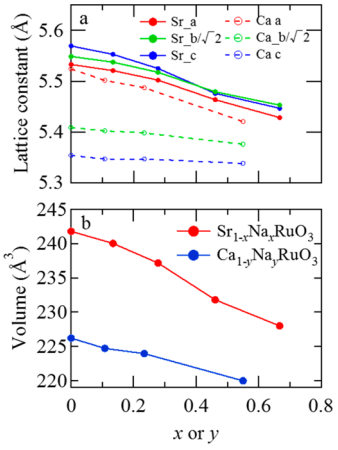

Figure 3. Changes in (a) lattice constants and (b) volume of $Sr_{1-x}Na_xRuO_3$ and $Ca_{1-y}Na_yRuO_3$ with changes in the Na doping x or y.

Ru−O bond length decreases and the Ru−O−Ru bond angle along the b axis also decreases slightly.

The temperature dependence of magnetic susceptibility measured at 1 kOe is shown in Figure 4a. As reported previously, $SrRuO_3$ (x = 0) shows a ferromagnetic transition at

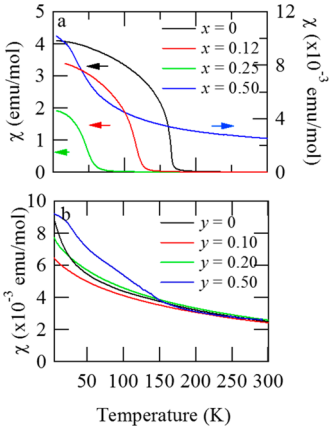

Figure 4. Temperature dependence of magnetic susceptibility measured at 1 kOe for (a) $Sr_{1-x}Na_xRuO_3$ (x = 0, 0.12, 0.25, and 0.50) and (b) $Ca_{1-y}Na_yRuO_3$ (y = 0, 0.10, 0.20, and 0.50).

dx.doi.org/10.1021/ic500265t | Inorg. Chem. 2014, 53, 4579−4584

160 K.[1] The magnetic transition temperature decreased with increasing Na substitution with both $x = 0.12$ and 0.25 showing a clear ferromagnetic transition at low temperatures. The inverse susceptibility ($1/\chi$) above the ferromagnetic transition temperature shows a linear Curie–Weiss-like behavior, and the Weiss temperature decreases from 165 K for $SrRuO_3$ to 30.7 K for the $x = 0.25$ sample (Figure 5). The magnetic behavior of

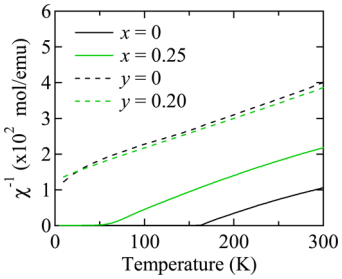

Figure 5. Temperature dependence of inverse susceptibility $1/\chi$ for $Sr_{1-x}Na_xRuO_3$ ($x = 0$ and 0.25) and $Ca_{1-y}Na_yRuO_3$ ($y = 0$ and 0.20).

the $x = 0.50$ sample is clearly different, and in this case there is no evidence for a ferromagnetic-like transition. It should be recalled that magnetic measurements are extremely sensitive to the presence of ferromagnetic species, and the absence of such features in the $x = 0.50$ sample shows that the magnetic properties are dominated by antiferromagnetic interactions. Clearly the ferromagnetic interaction between the Ru spins is suppressed by the Na doping. The $1/\chi$ vs temperature plot for the $x = 0.50$ sample is consistent with the sample being antiferromagnetic, although the phase separation evident in the diffraction data precludes analysis of this.

All the Na-doped samples show low resistivity, 10^{-3} Ω·cm, at room temperature. The resistivities are almost temperature independent and decrease slightly with decreasing temperature (Figure 6a), suggesting weak metal-like behavior. There is an

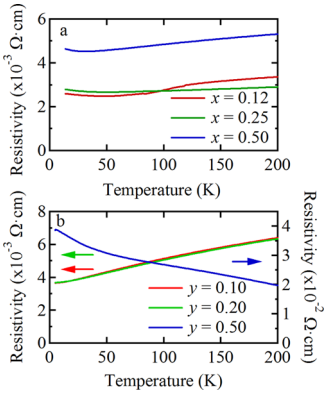

Figure 6. Temperature dependence of resistivity for (a) $Sr_{1-x}Na_xRuO_3$ ($x = 0.12$, 0.25, and 0.50) and (b) $Ca_{1-y}Na_yRuO_3$ ($y = 0.10$, 0.20, and 0.50).

obvious anomaly in the resistivity of the $x = 0.12$ sample near 100 K that is associated with the ferromagnetic transition. Similar magnetoelectric coupling was observed in pure $SrRuO_3$. The other two samples, with $x = 0.25$ and 0.50, do not display anomalies at T_C, although there is a slight upturn in the resistivity at low temperatures, possibly due to weak electron–electron interactions.

$Ca_{1-y}Na_yRuO_3$. Figure 1b shows the SXRD patterns of $Ca_{1-y}Na_yRuO_3$ ($y = 0.10$, 0.20, and 0.50). Splitting of the stronger Bragg reflections is clearly evident in this figure, and this, together with the presence of the appropriate superlattice reflections, demonstrated that each of the samples has a *Pnma* orthorhombic crystal structure. This was confirmed by Rietveld refinements that demonstrated the samples to be single phase. The refined Na occupancies for the $y = 0.10$, 0.20, and 0.50 samples of 0.108(7), 0.234(1), and 0.550(6) are in good agreement with the target compositions. Refinements in which the occupancy of the two anion sites was allowed to vary did not provide any evidence for the presence of anion vacancies. Unlike the $Sr_{0.5}Na_{0.5}RuO_3$ sample, $Ca_{0.5}Na_{0.5}RuO_3$ did not show phase separation and Na could substitute for up to at least 50% of the Ca in a single-phase sample. The structure analysis results for $Ca_{1-y}Na_yRuO_3$ are listed in Table 1, which show that these oxides have a large orthorhombic distortion, defined as the difference in the orthorhombic lattice constants, that decreases as the Na content is increased. The lattice constant a decreases while the lattice constants b and c are almost unchanged by Na doping, and as a result, the volume of the cell decreases (Figure 3b). The superlattice reflections associated with the octahedral tilting are considerably stronger in the Ca-containing compounds than in the analogous Sr oxides, reflecting the larger magnitude of the tilts. The orthorhombic *Pnma* structure is characterized by two independent octahedral tilts, ψ and φ, where ψ is an out-of-phase tilt about the pseudocubic 101 axis, and φ is an in-phase tilt about the pseudocubic 010 axis. The magnitude of these can be estimated by the displacement of the O2 oxygen atoms from 1/4 0 1/4. Doping of $CaRuO_3$ with Na reduces these from 15.6° and 15.1° to 13.9° and 13.3°, respectively, at $y = 0.50$. These changes in the tilts are reflected in the Ru–O–Ru angles that increase with Na doping in $Ca_{1-y}Na_yRuO_3$. It should be recalled that the Ru–O–Ru angles are dependent on both the anisotropy of the unit cell parameters and the magnitude of the octahedral tilts.

Figure 4b shows the temperature dependence of the magnetic susceptibilities measured at 1 kOe of the $y = 0.10$, 0.20, and 0.50 samples, and these are quite similar to that of the undoped $CaRuO_3$. The Weiss temperatures of the Na doping samples are slightly higher than that of $CaRuO_3$ (Figure 5), and no antiferromagnetic-like transition, like that reported for $Ca_{0.95}Na_{0.05}RuO_3$, was observed.[12] The $Ca_{1-y}Na_yRuO_3$ ($y = 0.10$ and 0.20) samples show low resistivity (10^{-3} Ω·cm) at room temperature, and their resistivity behavior is similar to that of the undoped $CaRuO_3$ (Figure 6b). The resistivity of $Ca_{0.5}Na_{0.5}RuO_3$ shows a semiconductor-like behavior, although the value at room temperature (2×10^{-2} Ω·cm) is not so high.

DISCUSSION

Na doping of $SrRuO_3$ and $CaRuO_3$ single crystals to yield $Sr_{0.88}Na_{0.12}RuO_3$ and $Ca_{0.95}Na_{0.05}RuO_3$ was reported previously.[13] A slightly more highly Na-doped ceramic, $Sr_{0.81}Na_{0.19}RuO_3$, was also reported, but we are unaware of further doping studies.[14] Attempts to prepare Na-doped $SrRuO_3$ and $CaRuO_3$ samples with higher doping concentrations at ambient pressure failed. Using high-pressure methods the limit of Na substitution in $SrRuO_3$ and $CaRuO_3$ was extended to 50%. The nominal $Sr_{0.5}Na_{0.5}RuO_3$ sample was not obtained as a single phase; rather phase separation to $Sr_{0.539(3)}Na_{0.461(3)}RuO_3$ and $Sr_{0.333(5)}Na_{0.667(5)}RuO_3$ occurred. The basis of this phase separation is not obvious, but it points to an upper solubility limit near $x = 0.7$. We can therefore

dx.doi.org/10.1021/ic500265t | Inorg. Chem. 2014, 53, 4579–4584

conclude that high-pressure synthesis enables Na to be substituted for over 50% of the Sr in $SrRuO_3$ and the Ca in $CaRuO_3$.

Na doping significantly decreases the volume of $SrRuO_3$. This is mainly attributed to the size effect of the substitution at the *A* site in the perovskite structure since for 12-fold oxygen coordination the ion radius of Na^+ (1.39 Å) is smaller than that of Sr^{2+} (1.44 Å). Surprisingly, the successful substitution of Na^+ with an ionic radius of 1.39 Å for Ca^{2+} (1.34 Å) resulted in a reduction in the volume of $Ca_{1-y}Na_yRuO_3$ as the extent of Na substitution increased (i.e., with increasing *y*). This is believed to be a consequence of partial oxidation of the Ru^{4+} that results in a decrease in the Ru−O bond length, as observed in both systems upon Na doping. The bond valence sum (BVS) for Ru calculated from the refined Ru−O bond lengths increases from 4.02 for the undoped $SrRuO_3$ to 4.53 for the $Sr_{0.333(5)}Na_{0.667(5)}RuO_3$ sample. Similarly, the Ru BVS increases from 3.93 ($CaRuO_3$) to 4.31 ($y = 0.50$). Thus, the results clearly indicate that the Na^+ substitution for Sr^{2+} or Ca^{2+} at the *A* site causes hole doping to Ru^{4+} at the *B* site. As found in the earlier experimental studies,[13] the three crystallographically unique Ru−O bond lengths are all reasonably similar; this experimental observation is a variance to the results of the recent computational studies.[20]

An interesting feature of the structural changes induced by the Na substitution is seen in the Ru−O−Ru bond angle along the *b* axis. In both systems the tolerance factor, defined as

$$t = \frac{r_A + r_O}{\sqrt{2}(r_B + r_O)}$$

where r_A, r_B, and r_O are the ionic radii for the *A*, *B*, and O ions, respectively, increases with Na doping (assuming partial oxidation of the Ru as the mechanism of charge balance rather than the formation of anion vacancies). This will lead to a decrease in the magnitude of the tilts, and the Ru−O−Ru angle should tend toward 180°. This effect is smaller in $Sr_{1-x}Na_xRuO_3$, reflecting the small rate of change in the tolerance factor. Although the volumes of both $Sr_{1-x}Na_xRuO_3$ and $Ca_{1-y}Na_yRuO_3$ samples decrease with increasing Na substitution, the Ru−O−Ru bond angle in $Ca_{1-y}Na_yRuO_3$ increases and that in $Sr_{1-x}Na_xRuO_3$ decreases (Table 1). This reflects the competing influence of changes in the tilting of the octahedra and in the lattice parameters.

Interestingly, the hole doping to Ru^{4+} does not cause significant changes in the resistivity behavior, although a slight increase in the resistivity at room temperature is observed. Computational studies suggest this is a result of a decrease in the number of electrons above the Fermi level and lowering of the density of states at the Fermi level.[20] Although $Ca_{0.5}Na_{0.5}RuO_3$ shows a semiconductor-like behavior, other samples still show metal-like behavior. The conductivity of $CaRuO_3$ can be tuned by both chemical substitution and, for epitaxial thin films, strain.[21,22] It is unclear if the observed metal−insulator transition is a consequence of hole doping or changes in the Ru−O−Ru overlap. An earlier study[13] reported insulating behavior of the $Sr_{0.88}Na_{0.12}RuO_3$ single crystal; however the present ceramic $Sr_{1-x}Na_xRuO_3$ samples all displayed metallic-like conductivity.

The magnetic properties are strongly influenced by substitution of Na for the Sr in $SrRuO_3$. The ferromagnetic transition temperature decreases from 160 K for $x = 0$ to 40 K for $x = 0.25$, and no transition was observed for the nominal $Sr_{0.5}Na_{0.5}RuO_3$ sample. Evidently the ferromagnetic interaction between the Ru spins is significantly suppressed by the Na doping, although it is unclear if this has resulted in a transition to an antiferromagnetic ground state, as observed in $SrTcO_3$.[15] Considering that $SrRuO_3$ with a Ru−O−Ru bond angle of about 160° shows ferromagnetic behavior while $CaRuO_3$ with a 153° Ru−O−Ru bond angle shows antiferromagnetic interaction, it is reasonable to postulate that a decrease in the Ru−O−Ru bond angle, induced by the Na substitution, should result in suppression of the ferromagnetic interaction in $Sr_{1-x}Na_xRuO_3$ by reducing the overlap of the Ru 4d orbitals. Such overlap will be further reduced by the oxidation of the Ru to the smaller Ru^{5+} state, and at the same time hole doping will reduce the filling of the 4d band. This systematic and appreciable reduction in the Curie temperature is consistent with an increase in the formal oxidation state of the Ru. Conversely, the magnetic properties of $Ca_{1-y}Na_yRuO_3$ are not significantly different from those of the undoped $CaRuO_3$, although the slight increase in the Weiss temperature is suggestive of a weakening of the antiferromagnetic interaction by the Na substitution. Since each substituted Na^+ ion generates one high-spin Ru^{5+} (t_{2g}^3 $S = 5/2$), it is necessary to consider both Ru^{4+} (t_{2g}^4 $S = 1$)−O−Ru^{5+} exchange and Ru^{4+}−O−Ru^{4+} exchange. Each isolated Ru^{5+} is likely to be coupled antiferromagentically to its six Ru^{4+} or Ru^{5+} neighbors in a G-type arrangement; however the precise strength of these interactions will be moderated by the local Ru−O−Ru angles. Deconvoluting the relative contribution of the three contributing effects, namely, the Ru−O−Ru bond angle, effective cation size, and band occupancy in $Ca_{1-y}Na_yRuO_3$ is beyond the scope of this work, but we note that the change in the magnetic interaction is also consistent with the change in the bond angle. Note again that no apparent antiferromagnetic-like transitions were observed in the present Na-doped samples.

CONCLUSIONS

Samples of $SrRuO_3$ and $CaRuO_3$ highly doped with Na were obtained. Although Na doping levels less than 20% have been previously reportedly by synthesis at ambient conditions, the present high-pressure synthesis enabled us to obtain $Sr_{0.333(5)}Na_{0.667(5)}RuO_3$ and $Ca_{0.450(6)}Na_{0.550(6)}RuO_3$. Structure analysis with SXRD data revealed that lattice constants of both $Sr_{1-x}Na_xRuO_3$ and $Ca_{1-y}Na_yRuO_3$ decrease with increasing Na doping, and the BVS results indicated hole doping to Ru^{4+} at the *B* site. Ferromagnetic interaction in the Na-doped $SrRuO_3$ was suppressed, probably because of a combination of a reduction in the Ru−O−Ru bond angle and a decrease in the number of electrons. The $Sr_{1-x}Na_xRuO_3$ oxides all showed metallic behavior, in contrast to the reported nonmetallic behavior observed in single-crystal samples. The Na-doping effects on the transport and magnetic properties of $CaRuO_3$ were insignificant. Although the clear antiferromagnetic peak was observed in the previous single crystal, no such clear antiferromagnetic behaviors were observed in the present $Ca_{1-y}Na_yRuO_3$.

AUTHOR INFORMATION

Corresponding Author

*E-mail: shimak@scl.kyoto-u.ac.jp.

Notes

The authors declare no competing financial interest.

dx.doi.org/10.1021/ic500265t | Inorg. Chem. 2014, 53, 4579−4584

■ ACKNOWLEDGMENTS

We thank D. Kan and N. Ichikawa for useful discussions. The synchrotron radiation experiments at SPring-8 were performed with the approval of the Japan Synchrotron Radiation Research Institute. This work was partly supported by Grants-in-Aid for Scientific Research (Nos. 19GS0207 and 22740227) and by a grant for the Joint Project of Chemical Synthesis Core Research Institutions from the Ministry of Education, Culture, Sports, Science and Technology of Japan. The work was also supported by Japan Science and Technology Agency, CREST. B.J.K. acknowledges the support of the Australian Research Council.

■ REFERENCES

(1) Randall, J. J.; Ward, R. *J. Am. Chem. Soc.* **1959**, *81*, 2629−2631.
(2) Noro, Y.; Miyahara, S. *J. Phys. Soc. Jpn.* **1969**, *27*, 518A−518A.
(3) Callaghan, A.; Moeller, C. W.; Ward, R. *Inorg. Chem.* **1966**, *5*, 1572−1576.
(4) Bouchard, R. J.; Gillson, J. L. *Mater. Res. Bull.* **1972**, *7*, 873−878.
(5) Kostic, P.; Okada, Y.; Collins, N. C.; Schlesinger, Z.; Reiner, J. W.; Klein, L.; Kapitulnik, A.; Geballe, T. H.; Beasley, M. R. *Phys. Rev. Lett.* **1998**, *81*, 2498−2501.
(6) Dodge, J. S.; Weber, C. P.; Corson, J.; Orenstein, J.; Schlesinger, Z.; Reiner, J. W.; Beasley, M. R. *Phys. Rev. Lett.* **2000**, *85*, 4932−4935.
(7) Tripathi, S.; Rana, R.; Kumar, S.; Pandey, P.; Singh, R. S.; Rana, D. S. *Sci. Rep.* **2014**, 4.
(8) Longo, J. M.; Raccah, P. M.; Goodenough, J. B. *J. Appl. Phys.* **2003**, *39*, 1327−1328.
(9) Goodenough, J. B. *Prog. Solid State Chem.* **1971**, *5*, 145−399.
(10) Gibb, T. C.; Greatrex, R.; Greenwood, N. N.; Kaspi, P. *J. Chem. Soc., Dalton Trans.* **1973**, 1253−1258.
(11) Cao, G.; McCall, S.; Shepard, M.; Crow, J. E.; Guertin, R. P. *Phys. Rev. B* **1997**, *56*, 321−329.
(12) Kiyama, T.; Yoshimura, K.; Kosuge, K.; Mitamura, H.; Goto, T. *J. Phys. Soc. Jpn.* **1999**, *68*, 3372−3376.
(13) Shepard, M.; Cao, G.; McCall, S.; Freibert, F.; Crow, J. E. *J. Appl. Phys.* **1996**, *79*, 4821−4823.
(14) Petr, T.; Karel, K.; Anke, W.; Jiří, H. *Solid State Sci.* **2010**, *12*, 1112−1120.
(15) Avdeev, M.; Thorogood, G. J.; Carter, M. L.; Kennedy, B. J.; Ting, J.; Singh, D. J.; Wallwork, K. S. *J. Am. Chem. Soc.* **2011**, *133*, 1654−1657.
(16) Rodriguez, E. E.; Poineau, F.; Llobet, A.; Kennedy, B. J.; Avdeev, M.; Thorogood, G. J.; Carter, M. L.; Seshadri, R.; Singh, D. J.; Cheetham, A. K. *Phys. Rev. Lett.* **2011**, *106*, 067201.
(17) Mravlje, J.; Aichhorn, M.; Georges, A. *Phys. Rev. Lett.* **2012**, *108*, 197202.
(18) Pi, L.; Maignan, A.; Retoux, R.; Raveau, B. *J. Phys.: Condens. Matter* **2002**, *14*, 7391.
(19) Izumi, F.; Momma, K. *Solid State Phenom.* **2007**, *130*, 15−20.
(20) Jiao, P.; Liu, Y.; Wang, X.; Chen, J. *Comput. Mater. Sci.* **2013**, *69*, 284−288.
(21) Rao, R. A.; Gan, Q.; Eom, C. B.; Cava, R. J.; Suzuki, Y.; Krajewski, J. J.; Gausepohl, S. C.; Lee, M. *Appl. Phys. Lett.* **1997**, *70*, 3035−3037.
(22) Maignan, A.; Raveau, B.; Hardy, V.; Barrier, N.; Retoux, R. *Phys. Rev. B* **2006**, *74*, 024410.
(23) Kobayashi, H.; Nagata, M.; Kanno, R.; Kawamoto, Y. *Mater. Res. Bull.* **1994**, *29*, 1271−1280.
(24) Bensch, W.; Schmalle, H. W.; Reller, A. *Solid State Ionics* **1990**, *43*, 171−177.